Granular Matter (2024) 26:50
https://doi.org/10.1007/s10035-024-01416-4

ORIGINAL REPORT

Scale-up of dry impregnation processes for porous spherical catalyst particles in a rotating drum: experiments and simulations

Pengfei Xu[1] · Yangyang Shen[1] · Bryant Avila[2] · Hernán A. Makse[2] · Maria S. Tomassone[1]

Received: 21 August 2023 / Accepted: 27 February 2024 / Published online: 30 March 2024

Abstract
Catalyst impregnation is the first step and one of the most crucial steps for preparing industrial catalysts. The process is typically performed in rotating vessels with a spray-nozzle to distribute the liquid onto porous catalyst supports until the pore volume is reached. The inter-particle variability of the impregnated liquid inside the particles significantly affects the activity and selectivity of the resulting catalyst. Current scale-up practices lead to poor fluid distribution and inhomogeneity in the liquid content. The aim of this work is to understand the dynamic behavior of the particles under the spray nozzle, which is essential for desired content uniformity, and to develop a scale-up model for the dry impregnation process. In this work, we considered four dimensionless numbers in the scaling analysis. The scale-up rules require that the dimensionless numbers are kept constant for different scales. Both DEM simulations and matching experiments of dry impregnation inside the porous particles were performed for different vessel sizes. The water content of the particles was compared for different times and locations, and the relative standard deviation is calculated from the axial water content. Simulation and experimental results show that particles achieve similar content uniformity at the end of impregnation, confirming that the scale-up rules are applicable to all vessel sizes. The dimensionless numbers give very good scale-up performance since curves collapse indicating similarity in the processes. In addition, the scale-up method is validated for different particle sizes in simulations.

Keywords Catalyst impregnation · Discrete element method · Rotating drum · Scale-up · Dimension analysis

1 Introduction

In the manufacturing of heterogeneous catalysts, impregnation is the process of a solution containing active metal components being added to the porous catalyst supports [1–3]. It is desirable to obtain a uniform fluid distribution and similar metal loading in each catalyst particle/pellet after the impregnation step. Impregnation is commonly conducted in a rotating vessel, while the metal solution is sprayed on the support particle [4]. Different processing equipment includes drums, V-blenders, and double cone blenders. It is crucial to be able to reproduce the same quality catalysts at the industrial scale after having the knowledge about the impregnation process at the laboratory and pilot scale. However procedures for catalyst manufacturing are usually developed in an empirical way, and current scale-up practices lead to poor fluid distribution and inhomogeneity in metal content.

The problem of scaling-up a batch process has long been a puzzle to all chemical engineers [5]. More than half a century ago, a principle of similarity was first proposed for the scale-up of any chemical or physical process [6]. One major prerequisite of this approach is that the physics of the process must be clearly understood [7, 8]. The application of dimensional analysis [9] is also common practice in the chemical industry and has been successfully implemented for the scale-up of power requirements for mixing equipment [10]. The method [11] involves producing dimensionless numbers and deriving functional relationships that completely characterize the process. Buckingham's pi theorem is then used to identify the number of dimensionless groups that characterize the process. Going from one size of the equipment to the next, the operating parameters are controlled so that the dimensionless numbers are kept

✉ Maria S. Tomassone
silvina@soe.rutgers.edu

[1] Department of Chemical and Biochemical Engineering, Rutgers, The State University of New Jersey, 98 Brett Rd. Piscataway, Rutgers, NJ 08854, USA

[2] Levich Institute and Physics Department, City College of New York, 10031 New York, USA

constant. In addition, geometrical and dynamic similarities are required to apply the dimensional analysis [11].

Numerous studies have been done on the scaling up of mixing and coating processes, such as powder blending [12, 13], wet granulation [14–17], and pharmaceutical coating [18–20] and spray drying [21], but none of these studies were performed in porous particles. In the area of powder mixing scale-up, Wang and Fan applied the principle of similarity and investigated the scale-up of tumbling mixers [12]. For the scale-up of dry-particle blending process, Muzzio et al. offered some simple guidelines for free-flowing and cohesive materials [13]. These studies do not account for the spray related processes. On the other hand, previous works on the scale-up of wet granulation mostly applied a dimensionless spray flux number [14, 15, 22]. Over the past decade, a number of researchers have investigated various factors that affect the pharmaceutical coating of drug tablets [23–34]. None of these studies mentioned above deals with porous particles.

It is crucial to highlight the distinct nature of our research. Our work significantly differs from the work mentioned in these references as it involves impregnation not merely on the surfaces of the particles but also within the pores of the particles, reaching up to a level of 98–99 percent pore volume filled with liquid. Our particles are inherently porous and filled with liquid in a manner that ensures the impregnation is carried out with precisely the amount of fluid required to fill the pores. This unique approach ensures that, once the system attains full saturation, the entire structure remains dry. For this reason the process receives the name of "dry" impregnation. The goal of this paper is to quantify the distribution of the fluid inside the particles in the particle bed and asses its uniformity.

Discrete element method (DEM) has been applied to investigate particle mixing and segregation [35], and to study the scale-up rules in mixers [36]. In our previous work [37, 38], an algorithm for the spray and inter-particle transfer of fluid onto and within a rotating bed of granular catalyst support was implemented to the DEM simulations. The simulations were validated by experiments utilizing a geometrically identical double cone blender fixed with a single nozzle impregnator.

It is crucial to be able to reproduce the same quality catalysts at the industrial scale after having the knowledge about the impregnation process at the laboratory and pilot scale. However procedures for catalyst manufacturing are usually developed in an empirical way, and current scale-up practices lead to poor fluid distribution and inhomogeneity in the metal content. In this work, we present a dimensional analysis and the dimensionless numbers used to characterize the scale up of the impregnation system. Section 3 contains the description of the simulation method. In Sect. 4 we present the experimental method which includes experiments in a small and large cylindrical vessel with validated simulations as well. These experimental results prove that the dimensionless numbers are good scale up parameters. In Sect. 5 we present a further proof that the dimensionless numbers are good scale up parameters using simulations on cylindrical slices of three different sizes. Finally the conclusions from the scale-up studies are presented in Sect. 6.

2 Dimensional analysis

We performed dimensional analysis on the impregnation process. Geometric and dynamic similarities are necessary to apply dimensional analysis. Two systems are considered similar if they are geometrically and dynamically similar. Geometrically similarity is represented by the same shape between different scales and the same ratio of characteristic linear dimensions. Dynamic similarity requires that the velocities and forces in all directions have the same ratio. Given the scale-up model, a number of key operation parameters, such as rotation speed and flow rate, can be predetermined to achieve controlled mixing and content uniformity across various scales. Dimensionless numbers are defined, and functional relationships are derived to completely characterize the process.

Extensive studies have been conducted on the scaling of rotating drums due to their simple geometry and wide application in the chemical and process industries as mixers, dryers, kilns and reactors. Ding et al. developed scaling relationships for rotating drums by non-dimensionalising the differential equations governing the behavior of solids motion [39]. The most relevant dimensionless groups include Froude number, drum geometric ratios, drum fill percentage and size distribution of the solid particles.

A cylindrical drum is considered as our impregnation vessel. A schematic of the vessel with a spraying nozzle is shown in Fig. 1. For this system, we considered 4 dimensionless numbers for scale-up analysis. All these quantities were derived taking into account that the system of different scales should have geometric and dynamic similarity. The dimensionless numbers were kept constant for different scales.

$\Pi_1 = \frac{L}{D}$, $\Pi_2 = \frac{A_{wetted}}{L^2}$, $\Pi_3 = Fr = \frac{\Omega^2 \times D}{2g}$, $\Pi_4 = C_Q = \frac{Q}{\Omega \times D^3}$

where L is the length of the cylinder, D is the diameter of the cylinder, A_{wetted} is the wetted area of the cylinder, Fr is the Froude Number, C_Q is the Flow Rate Number, Ω is the angular velocity (or rotational speed), and Q is the flow rate of spraying solution. Other researchers have designed similar dimensionless numbers. Ban et al. [34] defined a dimensionless number as $\frac{X_{center}}{D}$, which includes the spray

center location (X_{center}) and the diameter of the cylinder (D). We instead defined $\frac{A_{wetted}}{L^2}$. Additionally, the wetted area in their work is a square, but the wetted area in our case is circular. The calculation of each dimensionless quantity converts specific operation parameters into a term value, and by keeping the value fixed in all scales, we are able to derive the operation parameters from one scale to another scale.

For geometrically similar impregnators, the fill level ratio is also kept constant: $M_2 = M_1 \frac{D_2^2 \cdot L_2}{D_1^2 \cdot L_1}$. M is the loading mass, D and L is the diameter and length of the drum respectively.

Froude number gives the correlation between vessel size and rotational speed of the vessel. Within different *Fr* regimes, different types of bed motion have been identified, such as slipping, rolling and cascading. The rolling bed is preferred, providing favorable conditions for mixing and uniformity. For a given vessel size, if the rotational speed and Froude number are too small, the system does not move, and no mixing occurs. At large Froude numbers, the vessel rotates at high speed, causing particle collision and attrition, which are to be avoided during the impregnation process. An optimal regime of the Froude number can be found when the system shows the best mixing behavior, in the rolling regime.

The flow rate number (C_Q) compares the rate of spray droplets (Q) being deposited onto the particle bed and the rate of particle being refreshed at the bed surface. The latter is correlated with the rotational speed (Ω) and the vessel diameter (D). In general, smaller spray rates tend to give more homogeneous liquid distribution during and after the total liquid is sprayed, however the process takes longer times. Using larger spray rates, the spraying can be completed in shorter times, but the particles show less uniformity of the fluid content in the particle bed. An optimal value for the Flow Rate number allows the impregnation process to finish in an acceptable time frame, and the final product to have a uniform distribution of the metal solution. However the process conditions may be limited to the equipment settings.

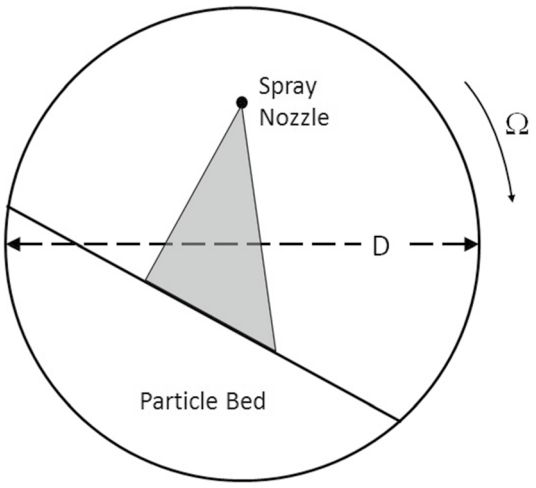

Fig. 1 A schematic of impregnation process in a rotating drum

3 Simulation method

Discrete element method (DEM) has been increasingly used to study granular materials and particle systems. In the DEM, the motion of individual particles is computed according to the Newton's second law of motion. The motion of a solid particle is expressed by

$$ma = \sum F_{Contact} + \sum F_{Body} \tag{1}$$

where m and a are the mass and acceleration of a solid particle, respectively. The term $\sum F_{Contact}$ accounts for all the normal and tangential contact forces, which are due to particle–particle or particle-boundary collisions. $\sum F_{Body}$ denotes the sum of all body forces due to gravity.

In our work we use DEM simulations using the EDEM commercial software package, developed by DEM Solutions, Ltd., which is based on an original method proposed by Cundall and Strack [40]. Our model also includes an additional water transfer algorithm that describes how the liquid is transferred inside the pellets.

The contact forces are calculated using Hertz-Mindlin no-slip contact model. It is based on a soft contact model or elastic approach, in which the magnitude of repulsive force is related of the amount of overlap. The normal force is calculated using a damped Hertzian normal contact model [41] with the damping term given by Tsuji et al. [42]. The magnitude F^n from a contact that resulted in a normal overlap δ_n is given by:

$$F^n = -k_n \delta_n^{3/2} - \gamma_n \dot{\delta}_n \delta_n^{1/4} \tag{2}$$

where k_n is the Hertzian normal stiffness coefficient, δ_n is the deformation (normal particle overlap), γ_n is the normal damping coefficient, and $\dot{\delta}_n$ is the rate of deformation. The time-dependent contribution $\dot{\delta}$ is the rate of overlap between particles, specifically addressing the normal overlap within the Hertzian Contact model. To delve deeper into the understanding of particle–particle and particle-geometry interactions, we can conceptualize them as a spring-dashpot system, where the normal force (F^n) is expressed as $F^n = F_{spring} + F_{damping.}$ The second half of this equation involves the dashpot or damping component, characterized by the rate of deformation $\dot{\delta}$. Eq. (2) represents the dashpot-damping component. This equation includes the time-dependent part, represented by the rate of deformation $\dot{\delta}$ which corresponds to the relative velocity between

two contacting elements. It is essential to note that the damping mechanics described above are an approximation within the dashpot-damping equation, and they offer a physically accurate representation of particle behavior when considering material coefficients of restitution. Further insights into the complex damping mechanics can be found in Colin Thornton's book [43].

In the above equation, k_n is obtained by:

$$k_n = \frac{4}{3} E_{eff} \sqrt{R_{eff}} \tag{3}$$

E_{eff} is the effective Young's modulus of two colliding entities (two particles or a particle and a wall). For entities with Poisson's ratios ν_1 and ν_2, Young's moduli E_1 and E_2, E_{eff} is given by:

$$E_{eff} = \frac{1-\nu_1^2}{E_1} + \frac{1-\nu_2^2}{E_2} \tag{4}$$

R_{eff} is defined as the effective radius of the contacting particles. In case of a particle–wall collision, the effective radius is simply the particle radius. While in the case of particle–particle collision, with the two contacting particles having radii R_1 and R_2, the effective radius is obtained by:

$$R_{eff} = \frac{R_1 \times R_2}{R_1 + R_2} \tag{5}$$

With knowledge of the normal stiffness coefficient and a chosen coefficient of restitution ε, the normal damping coefficient is calculated as:

$$\gamma_n = 2\sqrt{\frac{5}{3}\left[\frac{ln(\varepsilon) \times \sqrt{mk_n}}{\sqrt{ln^2(\varepsilon) + \pi^2}}\right]} \tag{6}$$

Following the work of Mindlin and Deresiewicz [44], the tangential force F^t is calculated in a similar method as its normal counterpart. The tangential contact force also consists of elastic and damping components. When a tangential overlap of δt is detected and there is a corresponding normal overlap of δn due to the same contact, then the tangential force is calculated as:

$$F^t = -k_t \delta_t - \gamma_t \dot{\delta}_t \delta_n^{1/4} \tag{7}$$

where k_t the tangential stiffness coefficient and γ_n is the tangential damping coefficient.

In the above equation, k_t is calculated by:

$$k_t = 8 G_{eff} \sqrt{R_{eff}} \sqrt{\delta_n} \tag{8}$$

G_{eff} is the effective shear modulus. For two entities with shear moduli G_1 and G_2:

$$\frac{1}{G_{eff}} = \frac{2-\nu_1}{G_1} + \frac{2-\nu_2}{G_2} \tag{9}$$

The tangential displacement (or overlap) δ_t is calculated by time-integrating the relative velocity of tangential impact, v_{rel}^t between two colliding entities (either interparticle or particle–wall contact):

$$\vec{\delta_t} = \int \vec{v_{rel}^t} dt \tag{10}$$

The capabilities of EDEM include user defined functions and various features for simulating impregnation process, which have been developed and validated in our previous work [17].

In the DEM simulations we employ two different vessels, 20Dx30L and 40Dx60L respectively. The vessel is initially filled with porous alumina catalyst particles, followed by the continuous release of liquid droplets from two nozzles located along the axis of the cylinder.

To account for the presence of fluid, our DEM model integrates an in-house code—a dedicated algorithm for fluid transfer that has been incorporated into the EDEM commercial code. This water transfer algorithm, successfully implemented in our previous papers [37, 38], employs discrete water droplets with a mass of 6.5×10^{-8} kg. Released from a nozzle, these droplets penetrate the pores of porous particles. The fluid transfer algorithm is explained in detail in our prior work in reference [37].

Upon contact, the liquid droplets vanish, transferring their water mass to the particles within the bed. Consequently, the mass of the support particles increases by the same amount as the mass of water transferred. This in consequence will affect the interaction between the particles since now the particles are heavier due the water inside their pores. The introduction of water into the pores of particles, rendering them heavier, inherently impacts the interactions between the particles. This modification is implicitly considered in Newton's equations within the Discrete Element Method's (DEM) governing equations. The added mass due to water absorption alters the dynamics of particle interactions, influencing forces, accelerations, and ultimately the overall behavior of the system. The DEM model, incorporating these changes, captures the complex interplay between particles with enhanced accuracy, reflecting the dynamic nature of the impregnation process.

To emulate the pore volume of the experimental catalyst, the catalyst support particles are assigned a predetermined threshold. If the absorbed liquid surpasses this threshold, the liquid transfer algorithm allows excess liquid on a specific catalyst support particle to be transferred to an adjacent

Table 1 Initial parameters and material properties used in the simulations

Parameter	Value
Density of particle	1500 kg/m^2
Diameter of particle	6.2 mm
Shear modulus	2×10^6 N/m^2
Poisson ratio	0.25
Coefficient of restitution	0.5
Coefficient of static friction	0.8
Coefficient of rolling friction	0.1

particle through particle–particle contact, governed by a user-specified rate.

In the simulations, various parameters were meticulously chosen to accurately replicate the experimental system. The material properties' values were directly sourced from the alumina catalytic support employed in the experiments, and these values are presented in Table 1 for reference, and the exact parameters used in experiments and simulations for the mass, speed and flow rates are indicated in Table 2.

4 Experimental method

Water impregnation experiments were conducted in two different cylindrical sizes: (1) A small cylinder (D1 = 20 cm and L1 = 30 cm) and (2) A large cylinder (D2 = 40 cm and L2 = 60 cm), mirroring the exact dimensions of the vessels used in the DEM simulations for a direct one-to-one comparison. Both systems were equipped with two spray nozzles positioned closely to each other, creating a continuous wetted area at the center of the vessel. Figure 2 illustrates the experimental setup for impregnation in the cylindrical vessels of both sizes. To maintain consistency, the rotational speed and spray rate were determined by keeping the Froude number (Fr) and Flow rate number (CQ) constant across the two scales. Following the completion of spraying, additional rotations were performed. Table 2 provides a comprehensive list of process parameters employed for the small and large cylinders. The chosen Froude number for both cylinders was $Fr = \frac{\Omega^2 \times D}{2g} = 0.0308$, and the flow rate number was $C_Q = \frac{Q}{\Omega \times D^3} = 6.54 \times 10^{-5}$.

It is essential to note that there is not a singular Froude number. In our scale-up studies, the approach involves the initial validation of simulation parameters through experiments. Subsequently, the chosen dimensionless numbers are scrutinized to confirm their suitability as effective scale-up parameters. These validation and verification steps will be presented in the following two sections after detailing the experimental setup.

Scale-up rules were used to determine the process parameters for a large vessel (D_2, L_2) based on those in a small vessel (D_1, L_1) using the Froude and flow rate numbers as Fr = 0.038, and $C_Q = 6.54 \times 10^{-5}$ respectively. Based on our chosen dimensionless numbers, we can observe that if the vessel size is increased by a factor of N (i.e. $\frac{D_2}{D_1} = \frac{L_2}{L_1} = N$), then the amount of material increases by cube of N (i.e. $\frac{M_2}{M_1} = N^3$), the wetted area increases by square of N (i.e. $\frac{A_{wetted,2}}{A_{wetted,1}} = N^2$), the rotation speed decreases by square root of N (i.e. $\frac{\Omega_2}{\Omega_1} = \sqrt{N}$), and the flow rate increases by N to the power of 2.5 (i.e. $\frac{Q_2}{Q_1} = N^{2.5}$).

4.1 Experimental setup

Experiments were carried out in both the small and large cylinders, with the vessel consistently loaded to a fixed fill level of 30% by volume. This fill level corresponds to 1.7 and 13.6 kg of alumina spheres for the small and large cylinders, respectively. 6.2 mm γ-alumina spheres were purchased from Saint-Gobain Norpro (Stow, OH, USA). The granular spheres contained a surface area of 200 m^2/g and a pore volume of 0.6 cm^3/g. An impregnator was retrofitted into

Table 2 Geometric parameters of the cylinders and process parameter used in the experiments and simulations (one to one correspondence)

Small cylinder	Large cylinder
$L_1 = 30$ cm	$L_2 = 60$ cm
$D_1 = 20$ cm	$D_2 = 40$ cm
Rotation speed Ω_1 **= 17 rpm**	Rotation speed Ω_2 **= 12 rpm**
Diameter of one Wetted area = 7.5 cm	Diameter of one wetted area = 15.5 cm
Mass $M_1 = 1.7$ kg	Mass $M_2 = 13.6$ kg
Volume of water = 1.01L	Volume of water = 8.01 L
Flow rate $\mathbf{Q_1 = 3}$ **L/hr**	Flow rate $\mathbf{Q_2 = 17}$ **L/hr**
Number of particles DEM:13,653	Number of particles DEM: 110,000
Time to run DEM: 3 months	Time to run simulations: 17.5 months
Fr = 0.038 $C_Q = 6.54 \times 10^{-5}$	Same dimensionless numbers

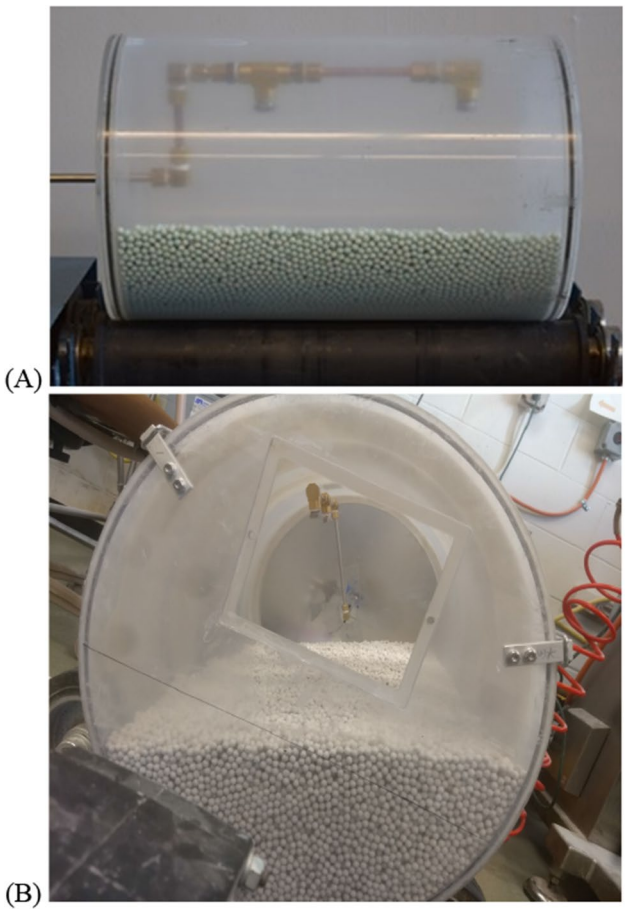

Fig. 2 Experimental set up for impregnation in a cylindrical vessel with 2 nozzles that are adjacent. **A** Small cylinder ($D_1 = 20$ cm and $L_1 = 30$ cm). **B** Large cylinder ($D_2 = 40$ cm and $L_2 = 60$ cm)

the system using Swagelok ¼ in. fittings and a ¼ inch NPT nozzle adapter. The flow was controlled using a Cole-Parmer Masterflex™ peristaltic pump retrofitted to the Swagelok fittings.

During the impregnation process, samples were retrieved every 5 min. The 6.2 mm spheres were removed for analysis at 5 points across the axis of rotation at the top of the bed. The sampling positions are shown in Fig. 3. Each sample contained approximately 20–25 particles. All samples were stored in air-tight glass vials prior to analysis for moisture. Moisture was analyzed by heating the samples to 300 °C for 6 h and measuring the associated mass change. Moisture content was normalized by the weight of the sample. The uniformity of the fluid inside the particle bed was characterized by the Relative Standard Deviation (RSD), which is defined as the ratio of the standard deviation of the water content among the particles inside the particle bed to the average content $\overline{C}$ representing the mean liquid content in the particle bed, as shown in Eq. (11). Equation (12) introduces $C_{i,}$ denoting the water content in each individual

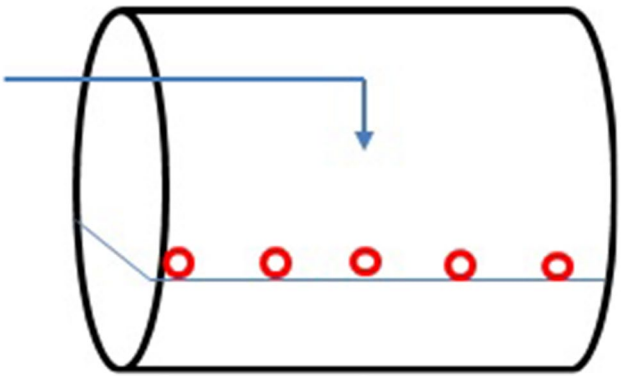

Fig. 3 Schematic of experimental set up and sampling positions along the rotational axis, shown as the red circles for both small and large cylinder

particle within the particle bed. The standard deviation is explicitly defined in Eq. (12).

$$RSD = \frac{\sigma}{\overline{C}} \tag{11}$$

and

$$\sigma = \sqrt{\frac{n\sum C_i^2 - \left(\sum C_i\right)^2}{n(n-1)}} \tag{12}$$

In general, lower RSD values indicate less variability between samples, which implies better mixing and fluid content uniformity. There is not a consensus regarding a fixed value for the relative standard deviation (RSD) uncertainty to indicate uniformity; rather, the value of the RSD used as a threshold depends on the application and the sample size [44]. In some cases, the observed variability is combined with the observed bias in the sample average to provide a combined criterion [30], so that the limit in RSD depends on the observed level of deviation in the sample mean. The size of our samples is about 20 to 25 particles per sample, and in each experiment, we tested 5 samples taken at five different times, with 3 repetitions, therefore a total of approximately 1500 units per experiment were tested, which provides enough measurements to yield a normal or near to normal distribution.

It is standard and widely accepted [45, 46] to consider a 95% or higher confidence interval in normal distributions to have assurance of batch acceptability. Our data show a 95% confidence interval (i.e. two standard deviations from the mean value taken at 100% pore volume filling) and our measurements of the RSD on those samples show RSD values that range from 0.09 to 0.109. Hence, we take RSD = 0.1 as our criterion for a reasonably good degree of uniformity since RSD values smaller than 0.1 correspond to a 95%

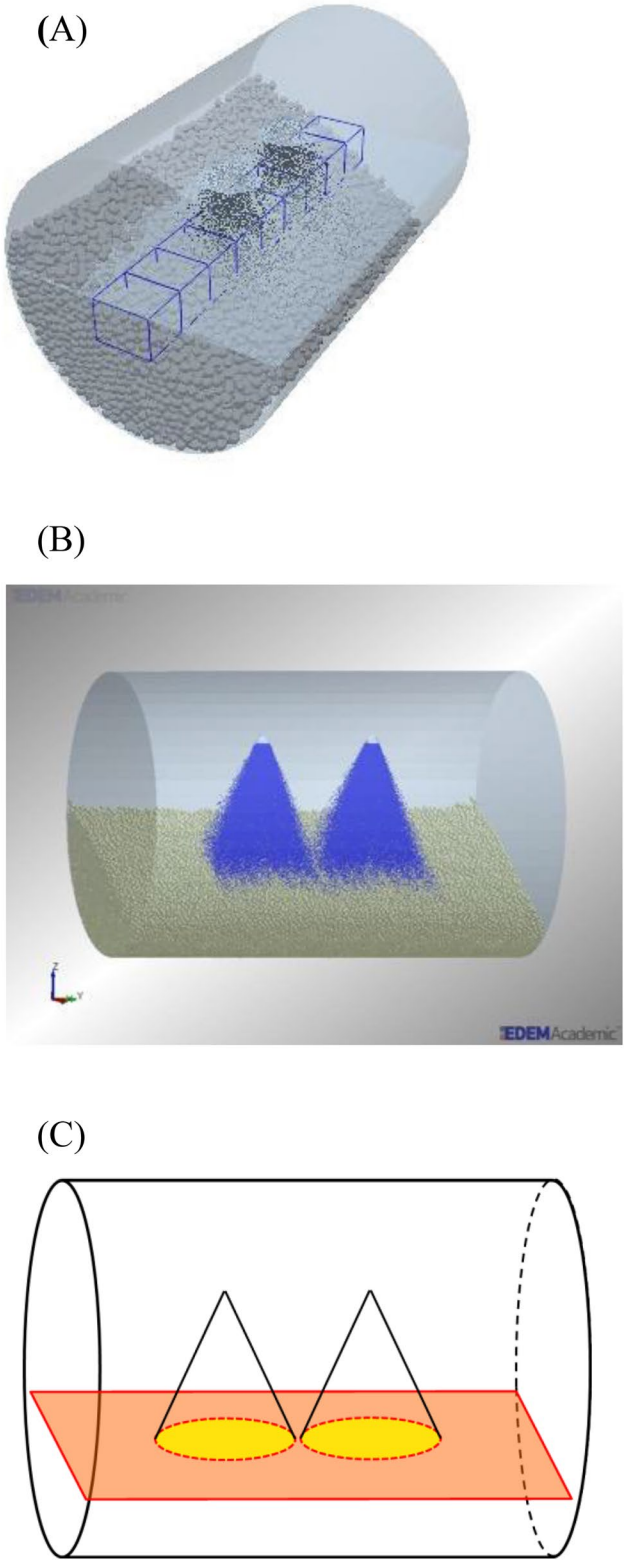

Fig. 4 **A** DEM simulation setup of the cylindrical vessel (D = 20 cm, L = 30 cm), 13,653 particles, m = 1.7 kg, 17 rpm, Q = 3 L/h, were used in these simulations. The boxes along the axial direction are the sampling points in the simulation. **B** DEM simulation with 110,000 particles in a 40Dx60L cylinder, mass = 13.6 kg, flow rate Q = 17 L/hr, rotational speed = 12 rpm, time to run simulations: 17.5 months; **C** schematic of the two nozzles in adjacent position in the cylinder

confidence interval. In addition, in general, in the catalysis industry it is widely accepted that a 10% variation in the catalyst quality is a reasonable variability, since other quality factors (surface area, activity, metals dispersion, crush strength, etc.) are often specified to this level of variation.

It is worth noticing that in this work, the RSD does not gauge mixing performance; rather, it assesses the uniformity of the liquid within the porous particles in the particle bed. The particles possess a dry surface but are filled with liquid up to 99 percent of their pore volume inside. Therefore, the RSD is measured with respect to the liquid inside the particles, not in terms of a specific location. We have previously published a paper [39] in which we discuss both the RSD for mixing and the RSD for fluid content uniformity. These two RSD values represent distinct concepts. In the current work, our focus is solely on assessing the uniformity of the fluid inside the particles, not the mixing of particles within the bed. Reference 39 demonstrated a robust correlation between mixing and fluid content uniformity in the particle bed. Mixing plays a crucial role in ensuring uniformity, implying that inadequate mixing leads to non-uniform distribution of fluid inside the particles throughout the entire particle bed.

4.2 Validation of DEM simulation parameters for both small and large cylindrical vessels

In order to validate the parameters chosen in the DEM model, we performed DEM simulations of water impregnation in cylindrical vessels with full length. Two sizes of vessel were considered: a small cylinder ($D_1 = 20$ cm and $L_1 = 30$ cm), and a large cylinder ($D_2 = 40$ cm and $L_2 = 60$ cm). Simulations and experiments have a "one to one" size correspondence (i.e. we kept the exact geometrical dimensions and nozzle configuration as compared to the ones used in experiments). Figure 4 shows the initial setup of the simulation and a schematic of the nozzle position for the small cylinder. The large cylinder has the same setup. Two nozzles are at the axial center of cylinder with the wetted area adjacent to each other. The DEM simulations for the small cylinder 20Dx30L are computationally very expensive due to the size of the vessel, we used 13,653 particles and each runs took 9 months to complete. Also notice that these simulations have axial dispersion. The particles used in the simulation have a uniform size of 6.2 mm.

The other operation conditions were the same as what were used in the experiments for both size cylinders. The details and geometric parameters are shown in Table 2. The water content in the particles were calculated in the 5 axial positions and compared the results with experimental results. The experiments were conducted in the small and large cylinders that have identical set up. Each experimental

point represents the mean value of three experiments; the error bars represent one standard deviation of the mean.

Figure 5 shows the comparison of the water content of the particles along the axial direction at different times for the small cylinder ($D_1 = 20$ cm and $L_1 = 30$ cm). Axial position is marked left to right by LL (far left), L (left), C (center), R (right), and RR (far right); temporal evolution begins at the bottom and increases vertically in 5 min intervals. It is important to note that the temporal evolution is represented by individual lines vertically, where each line represents 5 min of impregnation. During spraying, the axial water content in the particle bed is increasing under a steady speed as shown in Fig. 5A. The case of small cylinder exhibits some anisotropy in the initial 10 min of experiments, but it is improved to a more uniform profile by the completion of the 20 min impregnation. Good agreement is observed between simulations and experiments, indicating that the parameters chosen in the simulations are validated.

After the spraying is finished, additional rotations are performed in both simulations and experiments for another 5 min. Figure 5B shows the water content after additional rotations. The profile at 25 min shows very good uniformity after additional rotations. The patterns exhibited by the simulations and the experiments are similar, showing that water distribution reached a uniformed profile. This indicates the content uniformity can be further improved by additional rotations.

Figure 6 shows the comparison of the water content of the particles along the axial direction at different times for the large cylinder ($D_2 = 40$ cm and $L_2 = 60$ cm). In this case, the water content also shows some disturbance during the entire process of impregnation. This could be due to inconsistency in the sampling positions. Then after additional rotations, the water content exhibits better distribution in the axis at 35 min. A non-trivial amount of rotations may be required to reach the same level of uniformity exhibited by the small cylinder case. Good agreement is also observed between simulations and experiments, indicating that the parameters chosen in the simulations are validated for the large cylinder system.

Additionally, this agreement is evident in the parity plot shown in Fig. 7, where the experimental and simulation values for water content for both small and large cylinders are shown. These results suggest that the DEM model and chosen parameters were able to successfully describe the dry impregnation process. This allows us to move forward to study the scale-up of the impregnation process using DEM simulations.

The relative standard deviation (RSD) of the water content along the axis were computed and compared between simulation and experiment for both small and large cylinders. Figure 8 shows RSD as a function of time. The results of experiment were averaged between experiments and error

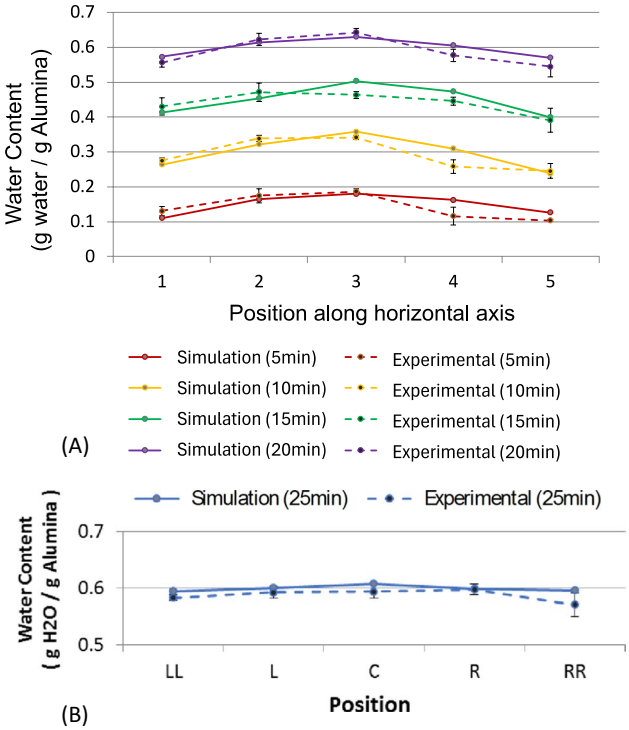

Fig. 5 Comparison between simulation and experiments of the axial water content distribution for the small cylinder ($D_1 = 20$ cm and $L_1 = 30$ cm) at different times. **A** during impregnation and **B** additional rotations

bars represent one standard deviation between three experiments. Good agreement between simulation and experiment is also evident in the comparison of RSD.

4.3 Verification that dimensionless numbers are good scale up parameters

To ensure that the two cylinders with different sizes exhibit similar performance in the uniformity of the fluid inside the particles in the particle bed, we measured the Relative Standard Deviation (RSD). RSD is calculated based on the water content inside the particles in the axial direction and is presented here as a function of time and the number of revolutions in Fig. 9. Figure 9A shows the plot of RSD as a function of time; revealing that the time needed for RSD to reach 0.1 is different for the small and large cylinders. Figure 9B displays the plot of RSD in relation to the number of revolutions. Notably, it is observed that both cylinders undergo the same number of rotations at the end of impregnation. Additionally, the two RSD curves collapse within the error bars, indicating that the dimensionless numbers serve as effective scale-up parameters across different scales.

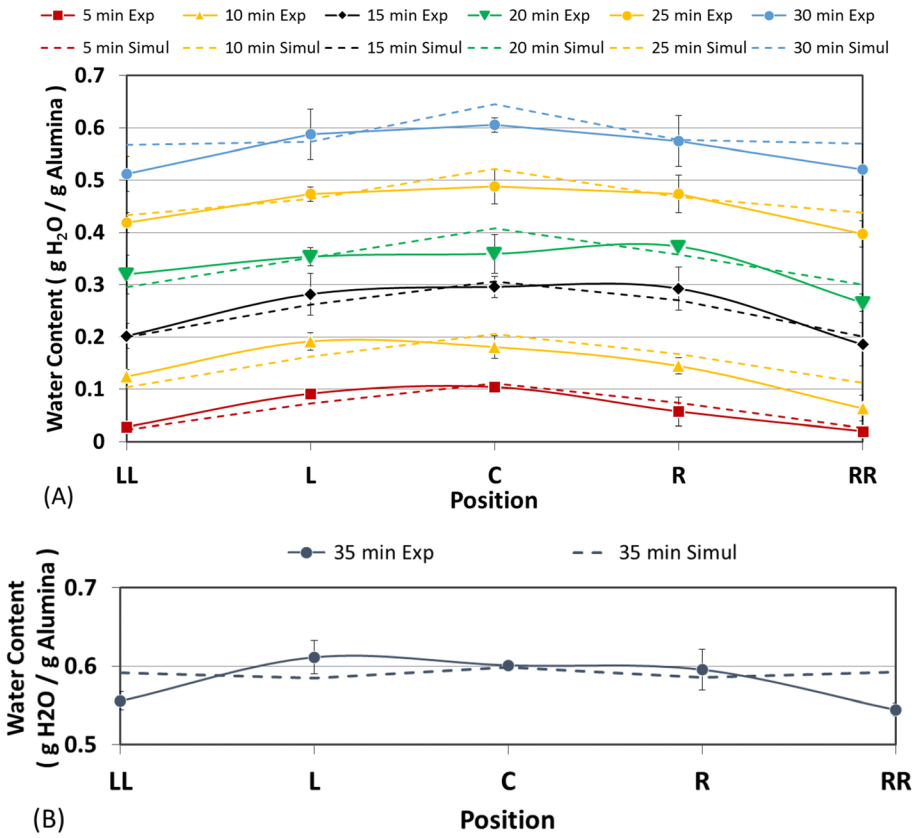

Fig. 6 Comparison between simulation and experiments of the axial water content distribution for the large cylinder ($D_2 = 40$ cm and $L_2 = 60$ cm) at different times. **A** during impregnation and **B** additional rotations

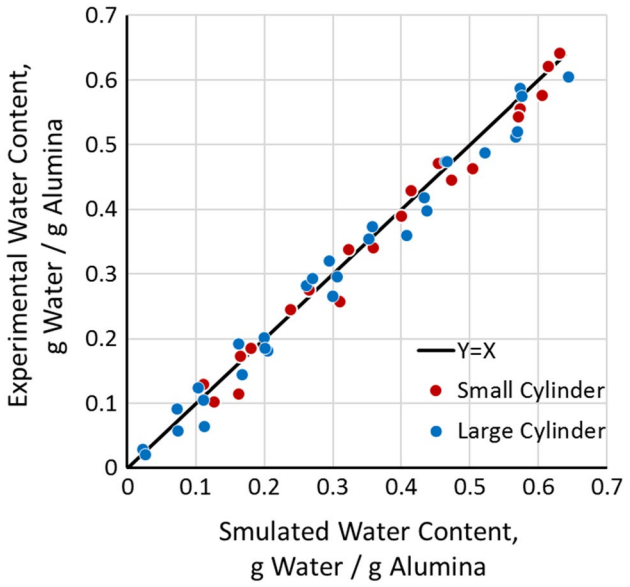

Fig. 7 Parity plot comparing the experimental values and computed values for the water content in the catalyst support particles. The results from both small and large cylinders are included

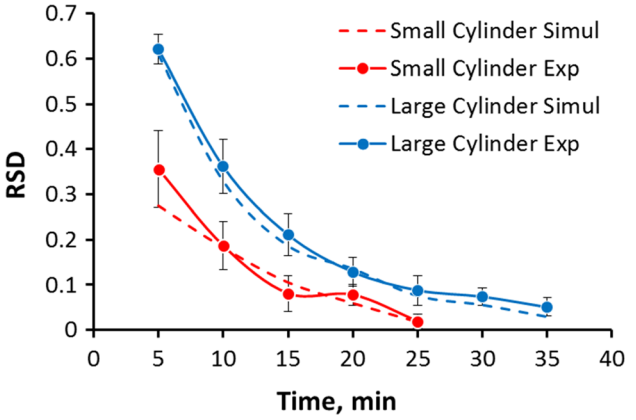

Fig. 8 Relative standard deviation of the axial water content as a function of time for both small and large cylinders

5 Simulation studies on scale-up

In order to further examine these dimensionless quantities, DEM simulations were performed in three sliced cylinders with different diameters with a width covering the entire spraying area. This geometry represents a portion in a cylindrical blender that includes 1 nozzle in the system. Note that the cylindrical slices with periodic boundary conditions are used in order to save computational time. The diameter of cylinder was varied from 10 to 20 cm, and 30 cm.

For all three sizes, the total number of particles in the system is determined to have the same fill level in the vessel, 30%. The rotational speed and spray rate are calculated from

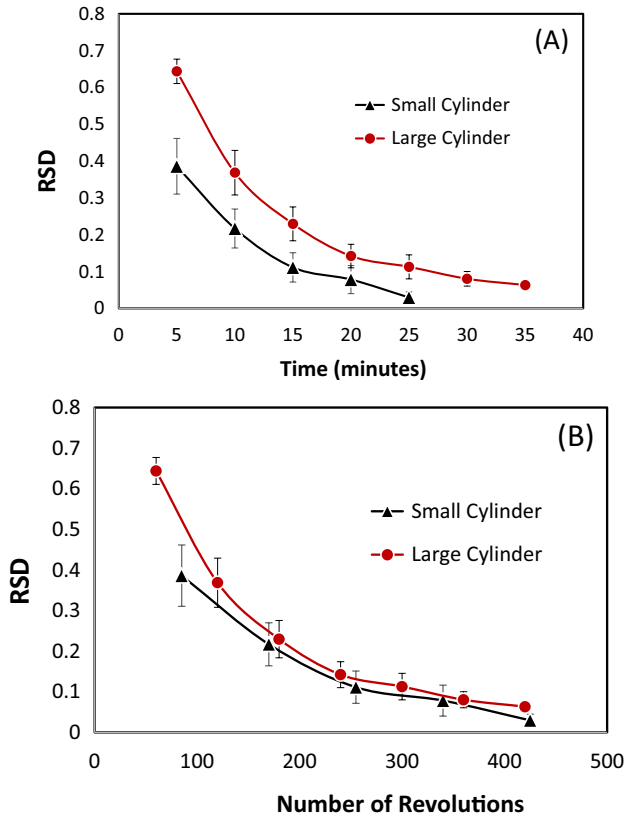

Fig. 9 Experimental RSD for small cylinder and large cylinder: **A** as a function of time and **B** as a function of number of revolutions

the Froude number (*Fr*) and the Spray Rate number (C_Q), respectively, $Fr = 0.009$ and $C_{Q=}0.00012894$. As the vessel size increases, the rotational speed decreases and the spray rate increases. The simulation conditions for different vessel sizes are given in Table 3. The initial setup of simulation is shown in Fig. 10.

Water content in the particles can be observed from simulation snapshots at different times during the impregnation process, as shown in Fig. 11. During the first 1 min, particles start to receive water from the spray nozzle and show a low water content in particles. Then particles keep adsorbing water and the water content increase with time. A small group of particles could have higher water content then the rest of the particles. At the end of spraying it is observed almost all the particles have similar water content, reaching to 100% pore volume filled. This is indicated by the redness across the particle bed. However, a small number of particles might have less than the complete saturation.

RSD is measured from the water content of all the particles in all three cylindrical slices. Firstly, the RSD is plotted as a function of time, as shown in Fig. 12A. It is observed that RSD reaches 0.1 at the end of spray for all sizes. The total amount of water needed to achieve complete pore filling is different for the different sizes; and as a result, the time

Table 3 Simulation setup for three different sizes of cylindrical slice

	Small slice $D_1 = 10$ cm $W_1 = 4$ cm	Medium slice $D_2 = 20$ cm $W_2 = 8$ cm	Large slice $D_3 = 30$ cm $W_3 = 12$ cm
Number of particles	$N_1 = 4000$	$N_2 = 8000$	$N_3 = 27{,}000$
Rotational speed (keeping Fr constant)	$\Omega_1 = 12.7$ rpm	$\Omega_2 = 9$ rpm	$\Omega_3 = 7.35$ rpm
Spray rate (keeping C_Q constant)	$Q_1 = 0.61$ L/hr	$Q_2 = 3.5$ L/hr	$Q_3 = 9.6$ L/hr

to finish the spraying is also different. The spraying time is dependent on the amount of material and the spray rate. Then RSD is plotted as a function of the number of revolutions, as shown in Fig. 12B. Using the same Froude number $Fr = 0.009$ and C_Q number $C_{Q=}0.00012894$, the RSD curves collapse into one curve. Similar performance is observed in the all three cylindrical slices. Thus, the dimensionless numbers can be used for system scale-up. The defined 4 dimensionless numbers are verified to fully scale up the system.

We investigated the optimization of the impregnation process, aiming to determine operational parameters for achieving uniformity in the shortest time. The relationship between vessel size and the rotational speed of the vessel is described by the Froude number. For a given vessel size, Fr is proportional to Ω^2 (i.e. $Fr = \frac{\Omega^2 \times D}{2g}$). Various bed motions, such as slipping, rolling, and cascading, have been identified in the literature within different Froude regimes [47].

The study conducted by Mellman and colleagues [47] revealed distinct behaviors of particles in a rotating drum in the absence of liquid inside the particles based on the Froude number (Fr). Specifically in ref [47] for completely dry particles in a rotating drum, the observed Froude number conditions were as follows:

(1) Slipping or cradling motion without mixing ($Fr < 10^{-4}$). In this regime, particles exhibited slipping motion without mixing. The low Froude number indicated that the centrifugal forces were not sufficient to overcome static friction, resulting in slipping rather than rolling or cascading.
(2) Rolling motion with mixing, $10^{-4} < Fr < 10^{-2}$. In this intermediate range of Froude numbers, particles engaged in rolling motion with effective mixing. The forces were adequate to overcome static friction, enabling particles to roll within the drum, leading to improved mixing.
(3) Cascading motion with mixing and crushing $Fr > 10^{-2}$. At higher Froude numbers, particles exhibited cascading motion with both mixing and crushing. The increased centrifugal forces allowed particles to cas-

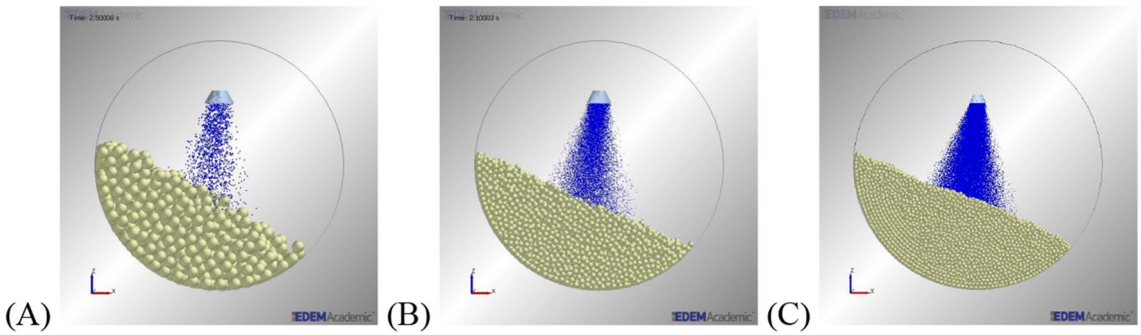

Fig. 10 Initial simulation setup of different sizes of cylindrical slice: **A** D = 10 cm, **B** D = 20 cm, **C** D = 30 cm

cade, leading to enhanced mixing. Additionally, the forces were sufficient to cause crushing, contributing to further particle interactions.

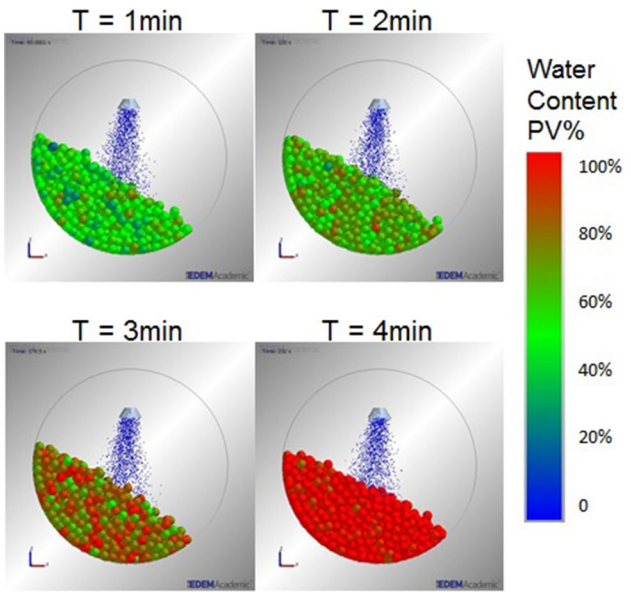

Fig. 11 Simulation snapshots of a cylindrical slice (D = 10 cm) at different times

To quantitatively assess these regimes, DEM simulations were initially conducted for a system in the absence of fluid, representing only particle mixing without impregnation. Subsequently, simulations were performed for a system in the presence of fluid, simulating a fully impregnated process.

In the first scenario, we examined a system without any fluid—solely involving the mixing of particles—at different speeds (0.5, 5, and 50 rpm) within a cylinder with a diameter of 30 cm and a width of 12 cm, while maintaining a 30% fill level. This resulted in low, intermediate, and high Froude numbers: $Fr_1 = 10^{-5}$, $Fr_2 = 4.2 \times 10^{-3}$. $Fr_3 = 0.42$.

Figure 13 illustrates the outcomes corresponding to these tested Froude numbers. Slipping/cradling motion was observed at speeds below 0.5 rpm, while rolling motion occurred within the speed range of 5 rpm < speed < 25 rpm. These findings align well with observations made in mixing studies in the absence of liquid [47].

Additionally, a more systematic study was conducted to identify the optimal Froude number in the presence of liquid for a dry impregnation process. This study utilized a sliced cylinder with a diameter (D) of 20 cm and a width (W) of 8 cm, employing a flow rate of 3 L/h.

Rotational speeds (Ω) were systematically varied from 1, 5, 10, 15, 20, 25, and 50 rpm, with the Froude number calculated as $Fr = \Omega^2 D/2g$. The Froude numbers, consequently go from 0.00011 to 0.279 as indicated in Fig. 14.

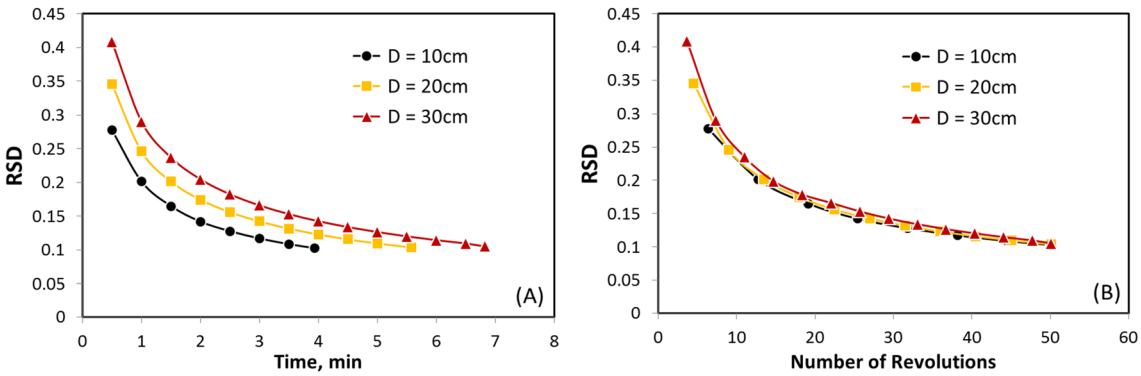

Fig. 12 RSD plots for different cylinder sizes: **A** as a function of time and **B** as a function of number of revolutions

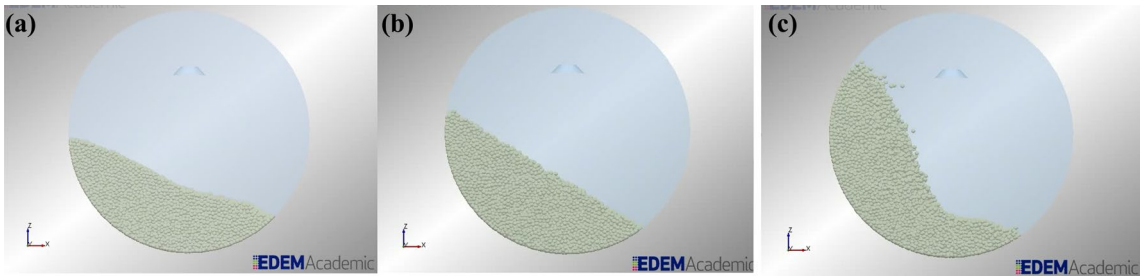

Fig. 13 DEM simulations snapshots of a cylindrical slide D = 30 cm, W = 12 cm in the absence of fluid, **a** slipping or cradling motion, at 0.5 rpm, Fr = 10^{-5}, **b** Rolling motion at 5 rpm, Fr = 4.2×10^{-3}, **c** Avalanching or cascading regime at 50 rpm, Fr = 0.42

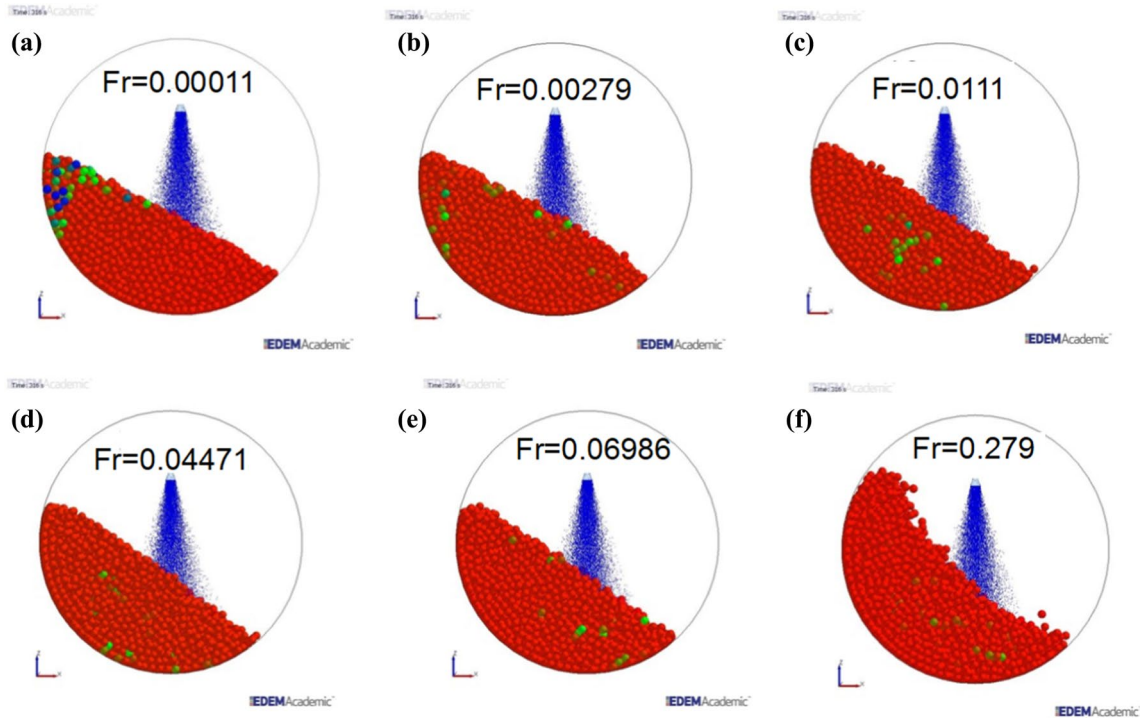

Fig. 14 Simulation snapshots at the end of spraying of a cylindrical slice (D = 20 cm) for different Froude numbers. At a Fr = 0.0001, a slipping regime is observed, for 0.00279 < Fr < 0.06986, the particle bed maintains a rolling regime. At higher Froude numbers (50 rpm, Fr = 0.279), a cascading regime is observed. The flow rate is constant at 3L/h

Maintaining a constant spray rate of 3 L/hr across runs with different rotational speeds (1–50 rpm) the flow rate numbers $C_Q = \frac{Q}{\Omega \times D^3}$ range from $C_Q = 1.98 \times 10^{-4}$ to $C_Q = 3.9 \times 10^{-5}$.

At the smallest rotational speed, 1 rpm, (Fr = 1.1×10^{-4}), a slipping motion is observed, where the particle bed moves with the rotating wall up to a certain angle, sliding back as a whole on the wall surface. This results in minimal particle mixing, and some particles remain dry or with a small amount of water, making this motion undesirable in practical applications.

For rotational speeds in the intermediate range, 10–25 rpm, 0.00279 < Fr < 0.06986, particles on the bed surface exhibit a uniform motion. The larger part of the particle bed is consistently transported upward with the rotating wall, resulting in a nearly leveled bed surface. The dynamic angle of repose is influenced by both rotational speed and fill level. This motion facilitates uniform and effective inter-particle mixing, producing particles with a consistent water content.

At the highest rotational speed, 50 rpm, Fr = 0.279, a cascading bed motion is observed, characterized by an arched bed surface typically featuring two angles. This motion leads to a reduction in the wetting zone area, and some particles detach from the bed, being thrown into free space. The high-velocity particles are prone to collisions, resulting in

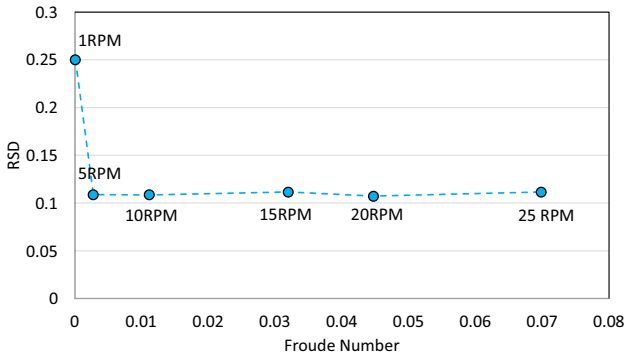

Fig. 15 RSD as a function of the Froude number for a system with a flow rate of 3L/h and D=20cm. There is a range of Froude numbers for which the value of the RSD is close to 0.1

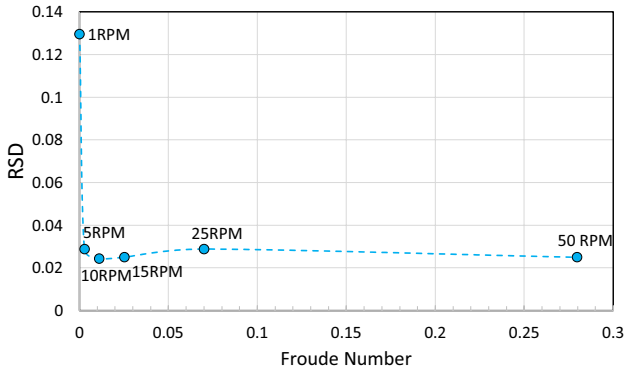

Fig. 16 RSD as a function of the Froude number for a system with a flow rate Q = 3.6 L/h and D=20cm. A range of favorable Froude numbers, with RSD values smaller than 0.1, spans from Fr = 0.00279 to Fr = 0.279, sig2 nifying good uniformity of the liquid inside the particle bed

particle collision and attrition—undesirable aspects during the impregnation process.

The Relative Standard Deviation (RSD) was calculated from the water content of all particles at the end of spraying. Figure 15 illustrates the RSD vs. the Froude number for various speeds of the vessel: 1, 5, 10, 15, 20 and 25 rpm. The RSD values were plotted as a function of the Froude number to identify the optimal Froude number for the impregnation process.

By inspection of Fig. 15 we observe that there is not a unique optimal Froude number for which RSD reaches a minimal value. We could argue that there is a "range" of good Froude numbers for which the RSD is near 0.1 that go from Fr = 0.00279 to Fr = 0.07.

To elucidate the effect of the flow rate, we performed simulations for the same size system (D = 20 cm and W = 8 cm) but for a different flow rate Q = 3.6L/h. The results are seen in Fig. 16.

Figure 16 shows the RSD values as a function of the Froude number for the same size system with a flow rate Q = 3.6 L/h. In this figure we can also observe a favorable range of Froude numbers (Fr) where RSD values are consistently below 0.1, ranging from Fr = 0.00279 to Fr = 0.279, indicating excellent uniformity of the liquid within the particle bed. Remarkably, a notable trend shows that increasing the flow rate in the same system gives much lower RSD values.

In these runs with a flow rate of 3.6L/h, the corresponding C_Q numbers that give good liquid uniformity are $C_Q = 2.38 \times 10^{-4}$ to $C_Q = 2.38 \times 10^{-5}$. Notably, it is observed that RSD values are lower when the flow rate is increased within the same system, as compared to the values presented in Fig. 15 at 3L/h.

Figure 17 depicts the RSD values vs. Froude numbers for a smaller cylinder (D = 10 cm, W = 4 cm) with a maintained flow rate of 3.6L/h. A range of favorable Froude numbers, where RSD values are consistently below 0.1, extends from

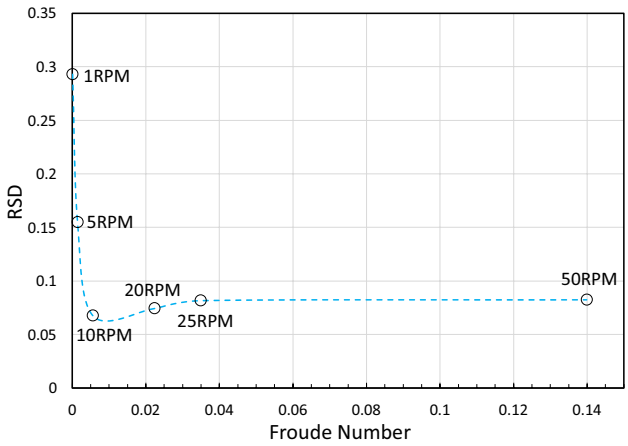

Fig. 17 RSD as a function of the Froude number for a cylindrical system with D = 10 cm and W = 4 cm, with a flow rate Q = 3.6 L/h

Fr = 0.00055 to Fr = 0.1398, indicating excellent uniformity of the liquid inside the particle bed. Notably, in the smaller cylinder, as it can be observed in Fig. 17, 1 rpm and 5 rpm do not yield good uniformity, both having RSD > 0.1. The optimal Froude numbers commence at 0.0055 and span up to 0.1398 for 50 rpm. It is noteworthy that at 50 rpm, despite good uniformity (RSD < 0.1) in this small system, there could be particle attrition due to cascading. The flow rate numbers for these runs are $C_Q = 9.5 \times 10^{-4}$ when Fr = 0.0055 and $C_Q = 1.9 \times 10^{-4}$ when Fr = 0.1398. We observe that this range of dimensionless numbers fall within the range of dimensionless number found for the larger system.

It is important to determine whether these results are contingent on the drum's geometry or its fill level. Intriguingly, drawing insights from our earlier findings concerning a double cone geometry at various fill levels (specifically, 30% and 45% fill levels) [37], where the Froude number and Flow rate

number were Fr = 0.08392 and $C_Q = 1.151 \times 10^{-5}$, respectively, we can argue that the Froude numbers and Flow rate numbers used for a different geometry and varied fill levels with optimal liquid uniformity inside the particle bed fall within the range observed in this systematic study. Hence the range found here does not depend on the geometry or the fill level. More studies are needed to elucidate the role of the pore volume of the particles.

In summary, there is not a single optimal Froude number that gives good uniformity. We cannot talk about "optimal" Froude without specifying the Flow rate and the pore volume of the particles. We observe that the flow rate Q and the pore volume of the particles have both an important effect on the final value of the RSD after spraying affecting the value of the optimal Fr. The range of optimal values for both C_Q and Fr extend from C_Q: $5.64 \times 10^{-5} < C_Q < 1.2 \times 10^{-4}$. and Fr: $0.00279 < Fr < 0.279$ independent of geometry and fill level.

Next, we examined the effect of particle size on the scale up performance. DEM simulations were performed in a cylindrical slice of D = 10 cm for different particle sizes (d = 2.5, 5, and 10 mm). The initial setup of simulations is shown in Fig. 18.

RSD is determined from the water content of all particles in each of the three cylindrical slices. Figure 19 illustrates RSD values as a function of the number of revolutions for various particle sizes within a fixed cylinder diameter and across different cylinder diameters. Initially, RSD begins with a larger value for smaller particle sizes, attributed to the slower mixing observed for smaller particles. However, uniformity can eventually be achieved after the same number of revolutions.

To investigate the effect of particle size on scale up, DEM simulations were performed for other cylinder sizes (D = 20 cm and 30 m) for the same particle sizes. In each particle size group, the operation conditions are determined by the scale-up rules. Figure 19B shows the RSD as a function of the number of revolutions. For each particle size group, RSD curves overlap with each other. The scale-up rules are applicable to any particle size group. Particle size does not appear to have a significant effect on the scale up. Ratios D/d = 10, 20, 40, 60, 80 do not seem to be affected. We did not use the size of the particles in any of the dimensionless numbers. There should be a ratio D/d for which scale up will break down.

6 Conclusions

We have developed a systematic approach for the scale-up of the impregnation process, employing four defined dimensionless numbers that effectively scale the entire system. Experimental impregnation trials in both small and large cylinders aligned well with our chosen Froude number within the optimal range predicted by simulations. The four selected dimensionless numbers demonstrated excellent scale-up performance, illustrated by collapsing curves indicating similarity in both geometric and dynamic aspects. The convergence of RSD curves into a single curve showcased consistent performance across various sizes. Validation of the scale-up method was achieved through a combination of simulations and experiments, and the application of our proposed scale-up rules to different particle sizes in DEM simulations exhibited good reproducibility.

However, it is important to note that our results were derived from a limited set of process conditions, specifically involving two sizes of cylindrical vessels and a single material type with a unimodal particle size distribution. The final product quality is primarily determined by mixing and dispersion, and issues may arise when applying the proposed dimensionless quantities to cohesive materials prone to poor mixing and agglomerate formation.

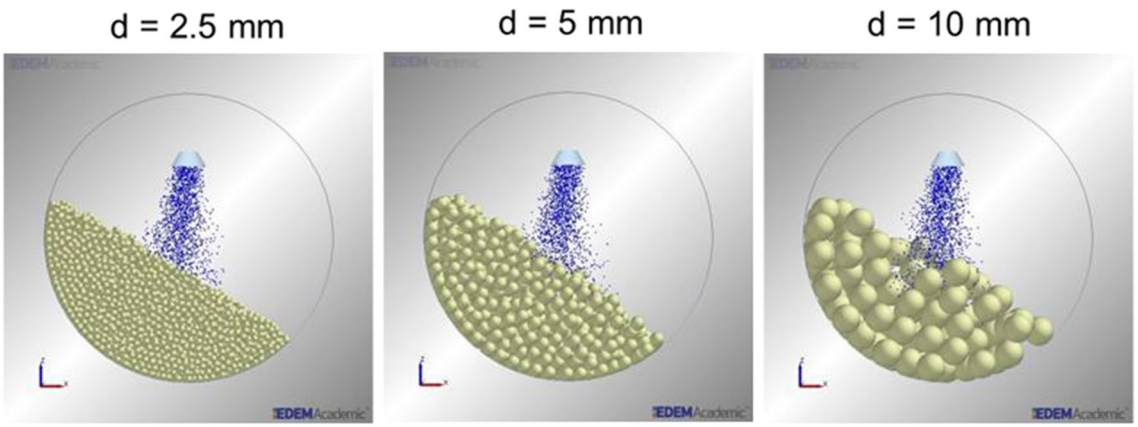

Fig. 18 Initial simulation setup of different particle sizes. The cylinder diameter is D = 10 cm

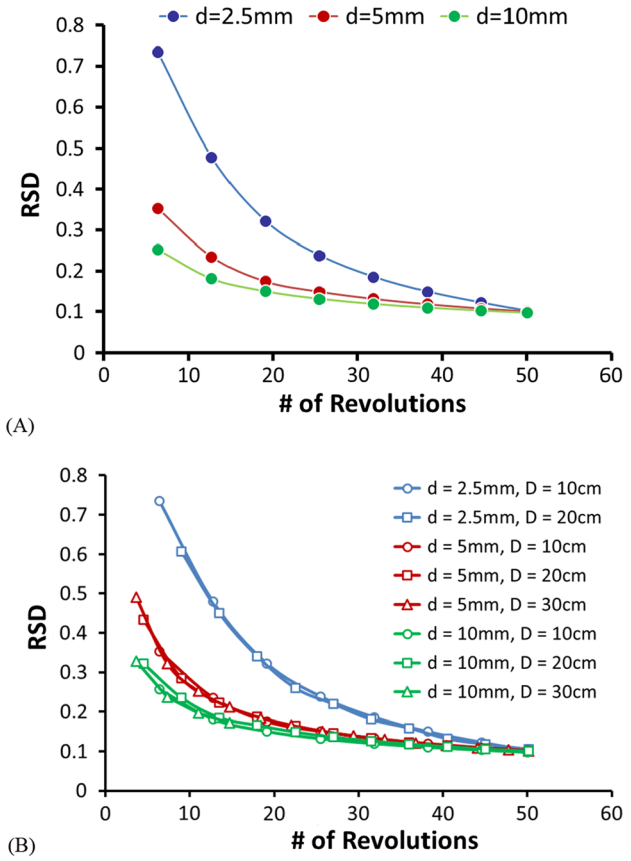

Fig. 19 RSD plot as function of number of revolutions for different particle sizes for **A** fixed cylinder diameter (D = 10 cm) and **B** different cylinder diameters

We observed that there is not a single optimal Froude number that guarantees excellent uniformity. We cannot discuss an "optimal" Froude without specifying the flow rate and the pore volume of the particles. We found that both the flow rate Q and the pore volume of the particles have a significant impact on the final value of the RSD in the impregnation of liquid inside the particles, thereby influencing the value of the optimal Fr and $C_{Q.}$ The range of optimal values for both C_Q and Fr extends from C_Q: $5.64\times10^{-5} < C_Q < 1.2\times10^{-4}$ and Fr: $0.00279 < Fr < 0.279$ independent of geometry and fill level. Further studies are needed to elucidate the role of the pore volume of the particles.

Future work is needed to assess the applicability of the scale-up rules to other materials. Furthermore, it is noteworthy that the derivation of dimensionless quantities in this study did not account for variations in particle size; instead, the dimensionless numbers were based on the size of the vessel and the total mass of the material. Therefore, future research should explore the impact of particle size on the proposed scale-up methodology. It would be also of interest to examine different particle size distributions in the future work.

Acknowledgements The authors would like to acknowledge the Rutgers Catalyst Manufacturing Consortium (RCMC) for funding and support. HAM acknowledges funding from NSF DMR- 1945909. We thank William Borghard for useful discussions and Deval Sharma, Matthew Borsellino, and Sai Sasidhar Guduru for their assistance with the research.

Declarations

Conflict of interest The author declares that he has no conflict of interest.

References

1. Schwarz, J.A., Contescu, C., Contescu, A.: Methods for preparation of catalytic materials. Chem. Rev. **95**(3), 477–510 (1995)
2. van Dillen, A.J., et al.: Synthesis of supported catalysts by impregnation and drying using aqueous chelated metal complexes. J. Catal. **216**(1–2), 257–264 (2003)
3. Barthe, L., et al.: Synthesis of supported catalysts by dry impregnation in fluidized bed. Chem. Eng. Res. Des. **85**(A6), 767–777 (2007)
4. Munnik, P., de Jongh, P.E., de Jong, K.P.: Recent developments in the synthesis of supported catalysts. Chem. Rev. **115**(14), 6687–6718 (2015)
5. Rossetti, I., Compagnoni, M.: Chemical reaction engineering, process design and scale-up issues at the frontier of synthesis: Flow chemistry. Chem. Eng. J. **296**, 56–70 (2016)
6. Johnstone, R.E. and M.W.: Thring, pilot plants, models and scale-up methods in chemical engineering. (1957).
7. Elson, T.: Scale-up in Chemical Engineering. In: Simons, S. (ed.) Concepts of Chemical Engineering 4 Chemists, pp. 171–202. The Royal Society of Chemistry (2007). https://doi.org/10.1039/9781847557674-00171
8. Zlokarnik, M.: Dimensional Analysis and Scale-up in Chemical Engineering. Springer Berlin Heidelberg, Berlin, Heidelberg (1991). https://doi.org/10.1007/978-3-642-76673-2
9. Zlokarnik, M.: Problems in the application of dimensional analysis and scale-up of mixing operations. Chem. Eng. Sci. **53**(17), 3023–3030 (1998)
10. Couper, J.R., J.R. Fair, W.R. Penney.: Mixing and agitation. Chemical Process Equipment: Selection and Design, 2010: p. 273-324
11. Levin, M.: How to scale up scientifically. Pharm. Technol. **2005**(1), S4–S11 (2005)

12. Wang, R.H., Fan, L.T.: Methods for scaling-up tumbling mixers. Chem. Eng. **81**(11), 88–94 (1974)
13. Muzzio, F.J., Alexander, A.W.: Scale up of powder blending operations. Pharm. Technol. **2005**(1), S34–S43 (2005)
14. Litster, J.D., et al.: Liquid distribution in wet granulation: dimensionless spray flux. Powder Technol. **114**(1–3), 32–39 (2001)
15. Hapgood, K.P., et al.: Dimensionless spray flux in wet granulation: Monte-Carlo simulations and experimental validation. Powder Technol. **141**(1–2), 20–30 (2004)
16. Boerefijn, R., Juvin, P.Y., Garzon, P.: A narrow size distribution on a high shear mixer by applying a flux number approach. Powder Technol. **189**(2), 172–176 (2009)
17. Pandey, P., Badawy, S.: A quality by design approach to scale-up of high-shear wet granulation process. Drug Dev. Ind. Pharm. **42**(2), 175–189 (2016)
18. Turton, R., Cheng, X.X.: The scale-up of spray coating processes for granular solids and tablets. Powder Technol. **150**(2), 78–85 (2005)
19. Pandey, P., Katakdaunde, M., Turton, R.: Modeling weight variability in a pan coating process using Monte Carlo simulations. AAPS PharmSciTech **7**(4), E2–E11 (2006)
20. Kariuki, W.I.J., et al.: Distribution nucleation: quantifying liquid distribution on the particle surface using the dimensionless particle coating number. Chem. Eng. Sci. **92**, 134–145 (2013)
21. Poozesh, S., Bilgili, E.: Scale-up of pharmaceutical spray drying using scale-up rules: a review. Int. J. Pharm. **562**, 271–292 (2019)
22. Litster, J.D.: Scaleup of wet granulation processes: science not art. Powder Technol. **130**(1–3), 35–40 (2003)
23. Pandey, P., Turton, R., Joshi, N., Hammerman, E., Ergun, J.: Scale-up of a pan-coating process. AAPS PharmSciTech **7**(4), E125–E132 (2006). https://doi.org/10.1208/pt0704102
24. Joglekar, A., et al.: Mathematical model to predict coat weight variability in a pan coating process. Pharm. Dev. Technol. **12**(3), 297–306 (2007)
25. Mueller, R., Kleinebudde, P.: Comparison of a laboratory and a production coating spray gun with respect to scale-up. AAPS PharmSciTech **8**(1), E21–E31 (2007). https://doi.org/10.1208/pt0801003
26. Prpich, A., et al.: Drug product modeling predictions for scale-up of tablet film coating-A quality by design approach. Comput. Chem. Eng. **34**(7), 1092–1097 (2010)
27. Just, S., et al.: Optimization of the inter-tablet coating uniformity for an active coating process at lab and pilot scale. Int. J. Pharm. **457**(1), 1–8 (2013)
28. Toschkoff, G., Khinast, J.G.: Mathematical modeling of the coating process. Int. J. Pharm. **457**(2), 407–422 (2013)
29. Agrawal, A.M., Pandey, P.: Scale up of pan coating process using quality by design principles. J. Pharm. Sci. **104**(11), 3589–3611 (2015)
30. Boehling, P., et al.: Simulation of a tablet coating process at different scales using DEM. Eur. J. Pharm. Sci. **93**, 74–83 (2016)
31. Boehling, P., et al.: Analysis of large-scale tablet coating: Modeling, simulation and experiments. Eur. J. Pharm. Sci. **90**, 14–24 (2016)
32. Dennison, T.J., et al.: Design of experiments to study the impact of process parameters on droplet size and development of non-invasive imaging techniques in tablet coating. PLoS ONE **11**(8), e0157267 (2016)
33. Suzuki, Y., et al.: A novel scale up model for prediction of pharmaceutical film coating process parameters. Chem. Pharm. Bull. **64**(3), 215–221 (2016)
34. Ban, J., et al.: Scaling inter-tablet coating variability in a horizontal rotating drum. AIChE J. **63**(9), 3743–3755 (2017)
35. Chaudhuri, B., et al.: Cohesive effects in powder mixing in a tumbling blender. Powder Technol. **165**(2), 105–114 (2006)
36. Nakamura, H., Fujii, H., Watano, S.: Scale-up of high shear mixer-granulator based on discrete element analysis. Powder Technol. **236**, 149–156 (2013)
37. Romanski, F.S., et al.: Dry catalyst impregnation in a double cone blender: a computational and experimental analysis. Powder Technol. **221**, 57–69 (2012)
38. Shen, Y.Y., Borghard, W.G., Tomassone, M.S.: Discrete element method simulations and experiments of dry catalyst impregnation for spherical and cylindrical particles in a double cone blender. Powder Technol. **318**, 23–32 (2017)
39. Ding, Y.L., et al.: Scaling relationships for rotating drums. Chem. Eng. Sci. **56**(12), 3737–3750 (2001)
40. Cundall, P.A., Strack, O.D.L.: A discrete numerical model for granular assemblies. Géotechnique **29**(1), 47–65 (1979). https://doi.org/10.1680/geot.1979.29.1.47
41. Hertz, H.: On the contact of elastic solids. J. Reine Angew. Math. **92**, 156–171 (1882)
42. Tsuji, Y., Tanaka, T., Ishida, T.: Lagrangian numerical-simulation of plug flow of Cohesionless particles in a horizontal pipe. Powder Technol. **71**(3), 239–250 (1992)
43. Thornton, C.: Granular Dynamics, Contact Mechanics and Particle System Simulations: A DEM study, Springer Cham, Softcover ISBN978–3–319–35454–5 Published: 22 October 2016. eBook ISBN978–3–319–18711–2Published: 03 September 2015, Series ISSN 1567–827X [https://link.springer.com/book/https://doi.org/10.1007/978-3-319-18711-2]
44. Mindlin, R.D., Deresiewicz, H.: Elastic spheres in contact under varying oblique forces. J. Appl. Mech. **20**(3), 327–344 (1953). https://doi.org/10.1115/1.4010702
45. *Guidance for Industry: Powder Blends and Finished Dosage Units — Stratified In-Process Dosage Unit Sampling and Assessment*. 2003; Available from: http://academy.gmp-compliance.org/guidemgr/files/5831DFT.PDF.
46. *<905> Uniformity of Dosage Units, The United States Pharmacopeial Convention*. 2011; Available from: https://www.usp.org/sites/default/files/usp/document/harmonization/gen-method/q0304_stage_6_monograph_25_feb_2011.pdf.
47. Mellmann, J.: The transverse motion of solids in rotating cylinders—forms of motion and transition behavior. Powder Technol. **118**(3), 251–270 (2001)